

Article

# Tidal Supplementary Control Schemes-Based Load Frequency Regulation of a Fully Sustainable Marine Microgrid

Hady H. Fayek <sup>1,\*</sup>  and Behnam Mohammadi-Ivatloo <sup>2,3</sup> 

<sup>1</sup> Electromechanics Engineering Dept., Faculty of Engineering, Heliopolis University, Cairo 11785, Egypt

<sup>2</sup> Faculty of Electrical and Computer Engineering, University of Tabriz, Tabriz 5166616471, Iran; bmohammadi@tabrizu.ac.ir

<sup>3</sup> Department of Energy Technology, Aalborg University, 9200 Aalborg, Denmark

\* Correspondence: hadyhabib@hotmail.com; Tel.: +20-1005472291

Received: 20 August 2020; Accepted: 24 October 2020; Published: 7 November 2020



**Abstract:** The world is targeting fully renewable power generation by the middle of the century. Distributed generation is the way to increase the penetration level of renewable energies. This paper presents load frequency control of a hybrid tidal, wind, and wave microgrid to feed an isolated island. This research is a step towards 100% renewable energy communities in remote seas/oceans islands. The wave and tidal generation systems model are presented. The study presents load frequency control through three supplementary control strategies: conventional integrators, fractional order integrator, and non-linear fractional order integrator. All the controllers of the microgrid are designed by using a novel black widow optimization technique. The applied technique is compared to other existing state-of-the-art algorithms. The results show that the black widow non-linear fractional integrator has a better performance over other strategies. Coordination between the unloaded tidal system and blade pitch control of both wind and tidal systems are adopted in the microgrid to utilize the available reserve power for the frequency support. Simulation and optimization studies are performed using the MATLAB/SIMULINK 2017a software application.

**Keywords:** marine microgrid; tidal generation system; black widow optimization; supplementary control; fractional integrator; non-linear fractional integrator; 100% renewable power generation

## 1. Introduction

The world is targeting 100% renewable power generation by the middle of this century [1]. Distributed renewable energy generation worldwide is increasing due to its low carbon dioxide emission and cost. The integration of renewable energies to the grid or high penetration level of renewables standalone systems suffers in terms of stability, power quality, and reliability [2]. Load frequency control plays an important role in terms of improving the power quality of the power systems, which operates with high variability in both loads and generation due to the presence of renewables [3].

Tidal energy is considered one of the promising renewable energy technologies in the 100% renewable energies dream. In [4], the researchers presented a feasibility study of tidal energy applications. Tidal power plants were always associated with offshore wind turbines to cover consumption needs. The integration of wind and tidal power plants to a grid or a power system were welcomed despite the frequency stability problems. With the increase of the penetration level of renewables in standalone systems and interconnected power systems, renewable energies must participate in the load frequency control process. The contribution is made in tidal and wind generators

by deloading. Deloading can be defined as the operation of the wind or tidal system at a power below the maximum power to create a reserve. The reserve can be utilized to stabilize the power system for frequency regulation during active power mismatch between generation and demand [5]. However, using deloading only cannot drive to the observed reduction in frequency deviation, but involving inertia and damping controls can reduce the reduction [6].

There are a lot of technologies to convert tidal energy into electrical energy. The best known technologies are barrages, turbines, and fences. In this paper, turbines technology is assumed to be used to convert tidal energy into a mechanical one. Through doubly-fed induction generators, the mechanical energy is converted to an electric one. In [7], the researchers presented a complete study on the dynamic behavior of pitch and stall regulated tidal turbines. In [8], the effect of integration tidal power plant on a real grid is discussed. Maximum power point tracking under different tides speed is presented in [9]. In [10,11], hybrid offshore wind tidal generating system is presented. Based on the literature review, there is not much focus on load frequency control by using the deloading of tidal generators. In this work, the deloading is applied by using inertia, damping, and various supplementary control schemes.

Wave energy has good potential in the 100% renewable power generation goal. It can satisfy more than 10% of the total global demand for electricity [12]. The structure of the Archimedes wave swing is presented in [13]. In this paper, wave energy was simulated as an uncontrollable generation system.

Control of microgrids is an important topic addressed by many researchers and applied using different optimization techniques. In [14], a particle swarm algorithm (PSO) is presented. In [15], a genetic algorithm (GA) is presented. In [16], the teaching and learning algorithm (TLBO) is presented, and in [17], harmony search is presented. The black widow optimization algorithm is presented for the first time in [18] by Hayyolalam and Kazem as a novel meta-heuristic approach for solving engineering optimization problems.

Load frequency control was previously applied by using different control schemes: proportional integral (PI) control [19], proportional integral derivative (PID) control [20], H-infinity [21], fractional order proportional integral derivative (FOPID) control [22], and non-linear proportional integral derivative (NPID) control [23]. The researchers proved the simplicity of PID, while better performance can be achieved through FOPID and NPID. In this paper, the supplementary control is designed to be a non-linear fractional integrator. At the same time, other controllers will be set to be PID to ensure both simplicity and quick response to a frequency deviation.

In [24], the research presents load frequency control of standalone tidal and diesel microgrid. The research presents a contribution through supplementary control from tidal generation to demand change.

In [25], the research load frequency control for wind-diesel generation microgrid using the D-partition method (DPM). The research provided a single step /simplistic computing method for calculating the PI controller parameters of a dynamic system, such as the microgrid system comprising of the renewable energy sources without any further requirements of retuning.

In [26], a novel fractional-order model predictive control technique is presented to track the optimal frequency of a standalone microgrid through including fractional-order integral cost function into model predictive control (MPC) algorithm.

In [27], In this research, a simulation and control of tidal generation system has been presented. A fuzzy system has been used for the pitch controller to properly modify the gains of the PID at different tidal inputs.

The main contributions of this paper are:

1. Simulation and control of a 100% renewable energy microgrid including tidal, wave and offshore wind hybrid generation system.
2. The effect of different supplementary control schemes in terms of the integrator, fractional integrator, and non-linear fractional integrator on the dynamic performance of load frequency control (LFC) is examined.

- Design of hybrid system controllers and tidal supplementary controller by using a novel black widow optimization technique and comparing it with other state-of-art optimization techniques.

The paper is organized as follows. Section 2 presents the modelling of the microgrid, Section 3 illustrates the applied control schemes. Section 4 presents the controller’s design process, Section 5 presents simulation results, and Section 6 is the main conclusion of this research.

## 2. Microgrid Modelling

The world is targeting 100% renewable energies by 2050. This paper presents a study on a standalone microgrid operated by fully sustainable marine generating systems, which are tidal, wind, and wave generators, as illustrated in Figure 1. The system’s mathematical descriptions are presented in the following subsections.

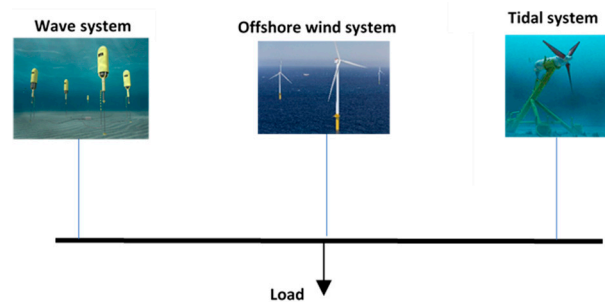


Figure 1. Marine microgrid.

### 2.1. Modeling of the Tidal Generating System

Both wind generating systems and tidal generating systems have similar operation and control principles. The difference between the two systems is that the tidal speed and nominal turbine size are less than for the wind. The wind rated speed ranges from 12–15 m/s and the tidal one from 2–3 m/s. The mechanical power output ( $P_T$ ) can be modeled as illustrated in (1) [4].

$$P_T = \frac{1}{2} \mathcal{P} A V^3 C_P(\gamma, \beta) \tag{1}$$

where  $\mathcal{P}$ ,  $A$ , and  $V$  are the seawater density, turbine blades area, and tidal speed flow, respectively;  $C_P$  is the power coefficient in terms of tip speed ratio ( $\gamma$ ) and blade pitch control angle ( $\beta$ ); while  $d_1, d_2, d_3, d_4, d_5, d_6$ , and  $d_7$  are  $C_P(\gamma, \beta)$  equation parameters.

$$C_P(\gamma, \beta) = \left( \frac{d_1 d_2}{d_6 \beta + \gamma} - \frac{d_1 d_7}{\beta^3 + 1} - d_1 d_3 \beta - d_1 d_4 \right) \exp\left( \frac{-d_5}{d_6 \beta + \gamma} + \frac{d_5 d_7}{\beta^3 + 1} \right) \tag{2}$$

$$\gamma = \frac{\omega R}{V} \tag{3}$$

Such that  $\omega$  and  $R$  are the rotational speed of the tidal blades and radius of the blades, respectively.

The tidal generating system has four modes of operation, as illustrated in Figure 2 and Table 1.

Turbine power variations are governed by the pitch control system comprising of a PID controller, which gets its input as error between measured turbine rotor speed and change in reference speed. The power varies with blade pitch control to what achieves the relationship between power output and rotor speed, as illustrated in Figure 2 [24].

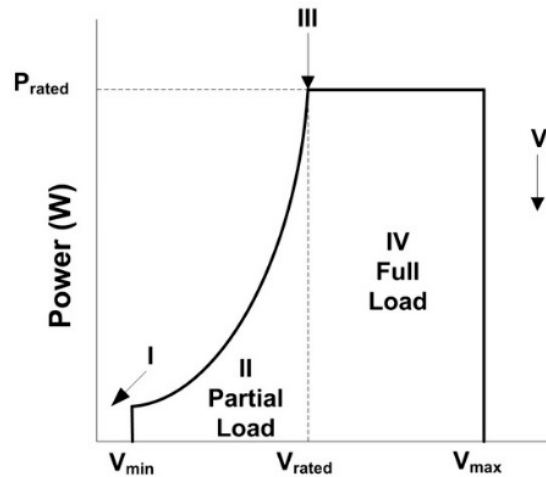


Figure 2. Tidal turbine modes of operation [24].

Table 1. Tidal turbine modes of operation [21].

Mode No.	Condition	Operation
I	$V \leq V_{min}$	No power generation with pitch angle setting 90 degrees.
II	$V_{min} < V \leq V_{rated}$	Optimum power extraction from the turbine to reach optimum efficiency, Blade pitch angle is set at 4 degrees in this work
III	$V_{rated} < V \leq V_{max}$	Constant power operation turbine, blade pitch angle is varied from 4 degrees to 90 degrees to avoid overload.
IV	$V > V_{max}$	No power output and blade pitch angle is set at 90 degrees.

Participation for frequency support is a must for 100% renewable generating systems. To ensure that tidal generating systems participate in frequency control, it is necessary to operate them at a level well below the maximum power point. This phenomenon is called deloading such that the power output of the system is varied between deloading power  $P_{del}$  and maximum power  $P_{max}$  as shown in Figure 3. This could happen by varying the rotor speed from deloading speed ( $\omega_{del}$ ) to nominal or rated speed ( $\omega_r$ ). The maximum deloading percentage  $x$  can be calculated based on the maximum allowed rotor speed for the generator, as illustrated in Figure 4.

$$P_{del} = (1 - x)P_{max} \tag{4}$$

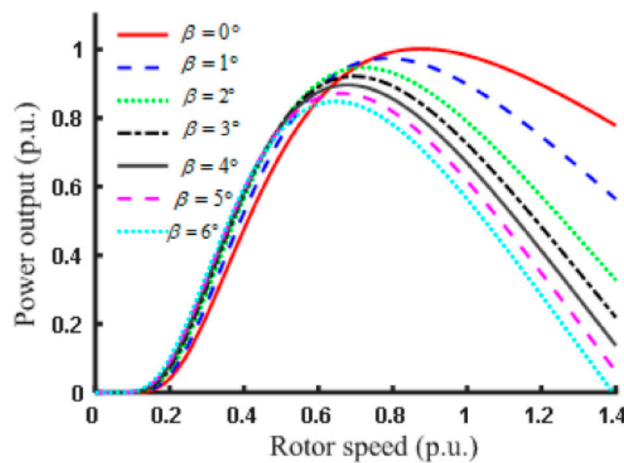


Figure 3. Tidal rotor speed vs. power output at different blade pitch angles [24].

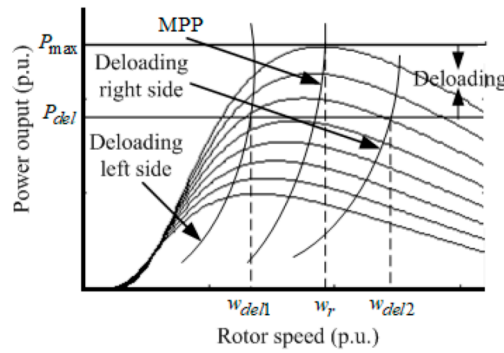


Figure 4. Deloading philosophy of tidal turbine [24].

Coordination between blade pitch control system and deloading system is required such that with the increase of the deloading percentage, the rotor speed may increase. At that instant, the blade pitch control system should adjust the blade pitch angle. The dynamic power reference ( $P_r$ ) at a specific rotor speed and reference speed ( $\omega_{ref}$ ) can be defined as:

$$P_r = P_{del} + (P_{max} - P_{del}) \left( \frac{\omega_{del} - \omega_m}{\omega_{del} - \omega_r} \right) \tag{5}$$

$$\omega_{ref} = \frac{P_r}{T_m} \tag{6}$$

where the measured mechanical torque is  $T_m$ .

To improve the frequency response, an additional signal  $\Delta P_{id}$  will be added to the reference power output, as shown in Figure 5. The additional signal is coming from combined inertia and damping non-conventional machine equivalent controller. In other words, the frequency deviation and rate of change of frequency are represented in two signals, as illustrated in (7).

$$\Delta P_{id} = -D_1 \Delta f - M \frac{\partial \Delta f}{\partial t} \tag{7}$$

where  $D_1$  and  $M$  are the additional damping and the additional inertia, respectively. To improve the response of the tidal system to the frequency deviation, different control schemes are compared to be added in parallel to  $D_1$  and  $M$ .

To drive the speed to track the reference speed, a PID control is applied, as illustrated in (8) and shown in Figure 6.

$$\Delta P_\omega = K_{\omega TP} \Delta \omega_e + K_{\omega TI} \int \Delta \omega_e dt + K_{\omega TD} \frac{d\Delta \omega_e}{dt} \tag{8}$$

where  $\Delta \omega_e$  is the error in speed deviation while  $K_{\omega TP}$ ,  $K_{\omega TI}$ , and  $K_{\omega TD}$  are the speed controller parameters. Thus, the change of the output power of the tidal generating system ( $\Delta P_{Tidal}$ ) can be formulated as (9).

$$\Delta P_{Tidal} = \frac{\partial P}{\partial \omega} \Delta \omega + \frac{\partial P}{\partial v} \Delta v + \frac{\partial P}{\partial \beta} \Delta \beta \tag{9}$$

where  $\frac{\partial P}{\partial \omega}$ ,  $\frac{\partial P}{\partial v}$ , and  $\frac{\partial P}{\partial \beta}$  are the change of tidal power with respect to the specific variation of turbine rotor speed, tidal speed, and blade pitch angle, respectively.

Tidal generating system parameters values are illustrated in Appendix A.

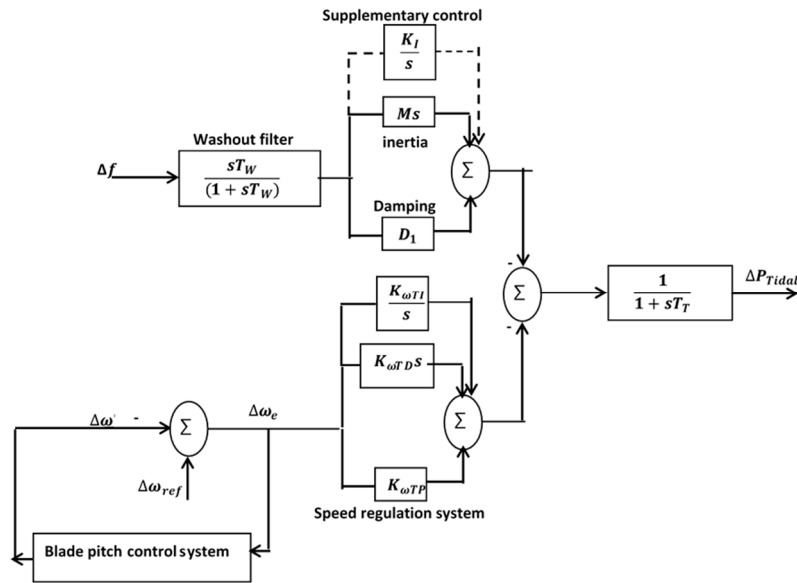


Figure 5. Tidal generation system model.

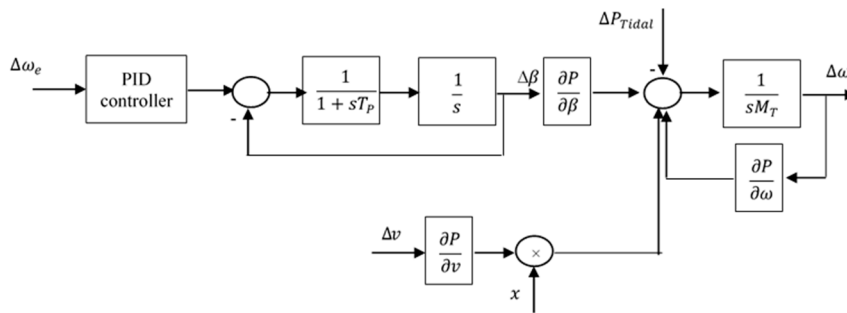


Figure 6. Blade pitch control of the tidal system.

2.2. Modeling of Wave Generating System

The wave generating system is one of the promising marine sustainable energy systems, which is not yet widely covered in the research. The wave system is assumed to be coupled with a permanent magnet synchronous generator. The following equations describe the dynamics of the system in terms of force ( $F_W$ ) and velocity ( $V_W$ ) [12,13].

$$V_W = \frac{dx}{dt} \tag{10}$$

$$F_W = m_{ft} \frac{dV_W}{dt} + (\beta_G + \beta_W)V_W + k_c x \tag{11}$$

where  $x$  is the floater and translator displacement,  $m_{ft}$  is the total mass,  $\beta_G$  is the damping constant of the generator, and  $\beta_W$  is the damping constant of the wave swing.

The system is simulated as a first-order generator, first-order converter, and first-order inverter, as illustrated in (12).

$$G_{wave} = \frac{K_{wave}}{1 + sT_{wave}} \frac{1}{1 + sT_{conv}} \frac{1}{1 + sT_{inv}} \tag{12}$$

where  $G_{wave}$  is the transfer function of the system, and  $K_{wave}$  and  $T_{wave}$  are the gain and time constants of the wave generator.  $T_{conv}$  and  $T_{inv}$  are the time constants of converter and inverter, respectively.

### 2.3. Modeling of Wind Generating System

The offshore wind generating system applied in this study is assumed to participate in frequency deviation by PID blade pitch control. The system is shown in Figure 7 and modeled in [22,25].

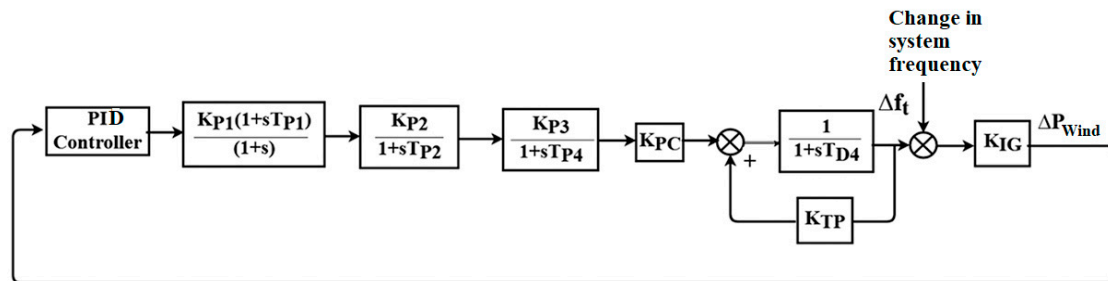


Figure 7. Offshore wind generating system.

### 2.4. Modeling of Microgrid

The microgrid is now formed from three marine systems. The change of the total generated power ( $\Delta P_G$ ) can be formulated as (13).

$$\Delta P_G = \Delta P_{Tidal} + \Delta P_{Wave} + \Delta P_{Wind} \tag{13}$$

The difference between the change in generation and the change in load is  $\Delta P_{Gd}$

$$\Delta P_{Gd} = \Delta P_G - \Delta P_D \tag{14}$$

The transfer function of the power system ( $G_{PS}$ ) in terms of changes in system frequency ( $\Delta f$ ) and  $\Delta P_{Gd}$  is illustrated in (15).  $D$  represents the frequency dependency of the load while  $H$  is the microgrid moment of inertia.

$$G_{PS} = \frac{\Delta f}{\Delta P_{Gd}} = \frac{1}{2Hs + D} \tag{15}$$

## 3. Controllers

### 3.1. Blade Pitch Controllers

Wind and tidal turbines have blade pitch controllers, which are selected to be proportional integral derivative (PID) controllers. PID controllers are the most widely used tool to minimize the error. The input of the PID controller is the error, and the output of the controller is the control action received by the actuators. Appropriate power injection is usually done through PID control, which usually leads to a minimum frequency deviation:

$$G_{PID} = K_P + \frac{K_I}{s} + K_D s \tag{16}$$

where  $K_P$  is the proportional gain,  $K_I$  is the integral gain, and  $K_D$  is the derivative gain.

### 3.2. Tidal Speed Controller

The tidal speed controller is selected to be PID controller, like the blade pitch controller.

### 3.3. Tidal Supplementary Control Schemes

Different tidal supplementary control schemes are applied to minimize the frequency deviation of the microgrid, which are as follows:

- (i) Integrators (I scheme), which have the transfer function  $G_I = \frac{K_I}{s}$

- (ii) Fractional integrators (FI scheme), which have the transfer function  $G_{FI} = \frac{K_I}{s^\lambda}$
- (iii) Non-linear fractional integrators (NFI), which have the output  $U_{NFI}(s) = \left( \frac{e^{(G \times E)} + e^{-(G \times E)}}{2} \frac{K_I}{s^\lambda} \right) E(s)$

where  $\lambda$  is the fractional-order operator of the integrator while  $G$  is the non-linearity gain,  $E$  is the error, and  $U_{NFI}$  is the output of the non-linear fractional integrator. Figure 8 shows the structure of NFI.

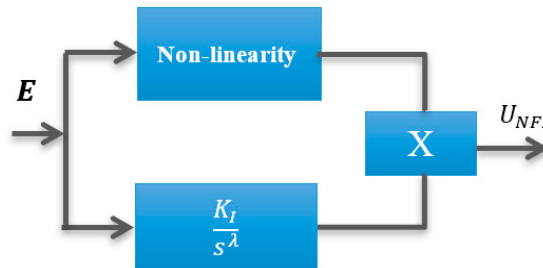


Figure 8. Non-linear fractional order integrator.

#### 4. Control Design

##### 4.1. Optimization Problem Definition

The design of wind and tidal turbines with blade pitch controllers, tidal speed controllers, and integrator based tidal supplementary control schemes will be performed for test operation condition using the following algorithms:

- i. Black widow
- ii. Quasi oppositional harmony search
- iii. Teaching and learning-based optimization
- iv. Particle swarm optimization
- v. Genetic algorithm

The best performance technique will be used for the rest of the subjected disturbances. The design is made in MATLAB to minimize frequency deviation. The optimization problem is described as follows:

- Objective Function (O): Minimization of integral absolute error (IAE) ( $O_1$ ) and minimization of integral time absolute error (ITAE) ( $O_2$ ):

$$O_1 = \min \int_0^T \Delta f \, dt \tag{17}$$

$$O_2 = \min \int_0^T t * \Delta f \, dt \tag{18}$$

$$O = 0.5 * O_1 + 0.5 * O_2 \tag{19}$$

- Variables: PID control parameters, tidal additional damping, and inertia, in addition to tidal supplementary control schemes parameters.
- Constraints:  $G$  and  $\lambda$ .

The multi-objective function is established such that weights of the ITAE and IAE are equal. The tidal supplementary control schemes parameters differ from one to another. In fractional integrators, there are two variables ( $K_I$  and  $\lambda$ ) and the constraint considered in its design is  $0 \leq \lambda \leq 1$

only. In non-linear fractional integrators, there are three variables ( $K_I$ ,  $G$ , and  $\lambda$ ) and the constraints considered are  $0 \leq \lambda \leq 1$  and  $0 \leq G \leq 1$  only.

#### 4.2. Black Widow Optimization

Recently, due to the complexity of renewable energy-based power systems, the need for a viable meta-heuristic method has emerged. Nature-inspired optimization algorithms are used widely for solving power system problems in an easy and flexible way. Their method is inspired by the unique mating behavior of the black widow spider. The proposed optimization technique includes the cannibalism stage, which omits inappropriate fitness from the selection circle, so that convergence comes earlier. Figure 9 illustrates the proposed algorithm steps, which are:

1. Initial population: This is used in each optimization technique; it has other names, like chromosomes in the genetic algorithm and particle position in the particle swarm algorithm. In the black widow, it has the name widow. To start the optimization, a candidate widow matrix with size  $N_{pop} \times N_{var}$  is generated, where  $N_{var}$  represents the solution of the problem array while  $N_{pop}$  represents the number of populations.
2. Procreate: In this step, an array called  $\alpha$  is created such that the offspring is produced through (20) and (21):

$$y_1 = \alpha \times x_1 + (1 - \alpha) \times x_2 \quad (20)$$

$$y_2 = \alpha \times x_2 + (1 - \alpha) \times x_1 \quad (21)$$

where  $x_1$  and  $x_2$  are parents, while  $y_1$  and  $y_2$  are offspring. The process repeated every  $\frac{N_{var}}{2}$ .

3. Cannibalism: There are three kinds of cannibalism: (a) sexual cannibalism, where the female black widow eats her husband; in the algorithm, we can identify male and female through their fitness function; (b) sibling cannibalism, where the strong spider siblings eat their weaker siblings; in the algorithm, the cannibalism rating is set according to the determined number of survivors; and (c) baby cannibalism, where baby spiders eat their mother; in the algorithm, strong and weak spider siblings are recognized through fitness value.
4. Mutation: Random selection of Mutepop number of individuals. Mutepop is calculated according to the mutation rate.
5. Convergence: The same concept of many algorithms comes in the proposed algorithm; three stop conditions may be used: (a) a predefined number of iterations; (b) the fitness value is almost constant for several iterations; and (c) the desired accuracy is reached.

Three parameters must be set for obtaining the desired results: procreating rate (pp), cannibalism rate, (CR) and mutation rate (pm). In this research, the parameters are selected as pp = 0.62, CR = 0.46, and pm = 0.4.

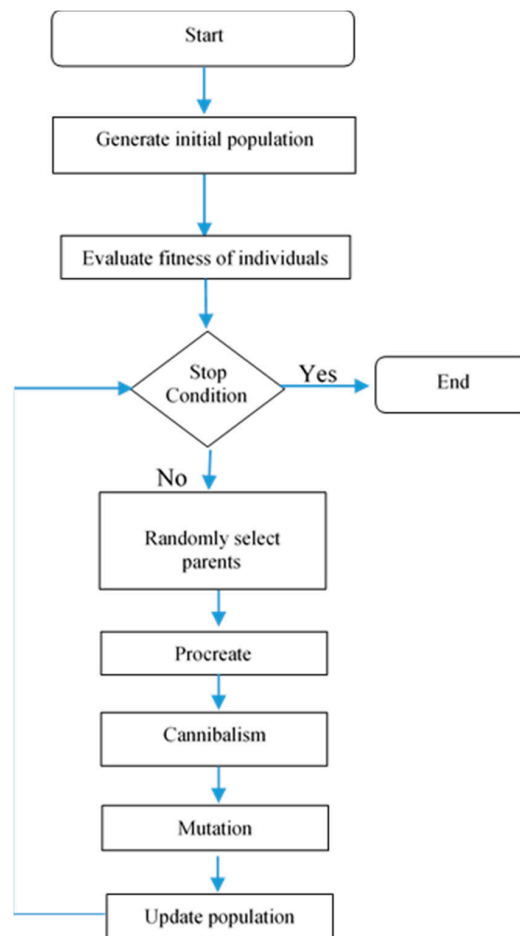


Figure 9. Black widow flow chart.

## 5. Simulation Results

In this part, the dynamic performance of the microgrid in terms of load frequency control is presented under different operating conditions. It is assumed that the tidal system is operating at tide speed 2.4 m/sec having a deloading effect with a 30° blade pitch control angle. The microgrid is simulated and optimization processes are applied on MATLAB/SIMULINK 2017a works in a Core i5, 2.50 GHz Samsung laptop with 6 GB of RAM. The parameters of all controllers in the wind and tidal systems are optimized using black widow optimization and its code is established using MATLAB 2017a. In order to establish the supremacy of black widow for the present work, system performance for 1% step load increase using integrator tidal supplementary control scheme is compared to other state-of-the-art optimization methods. Figures 10–12 show the frequency deviation, change in tidal power, and change in wind power. Table 2 shows a comparison between the performance of each optimization technique on ITAE, IAE,  $\int(\Delta f)^2$ , transient response of  $\Delta f$  in terms of undershoot ( $U_{sh}$ ), overshoot ( $O_{sh}$ ), settling time ( $t_s$ ) in addition to peak time ( $t_p$ ), and the number of iterations performed using each optimization technique. The results show that the black widow algorithm has the best performance over other algorithms. Therefore, the tests applied on the system to compare between different supplementary controllers will be applied using the black widow algorithm only. The dynamic study of the microgrid in terms of load frequency control, under the action of black widow tuned control schemes installed in the studied system, was subjected to the following tests:

*Test 1: A step increase in the demand;*

*Test 2: Real demand variation at a certain day;*

*Test 3: Sinewave variation of the wave generation system;*

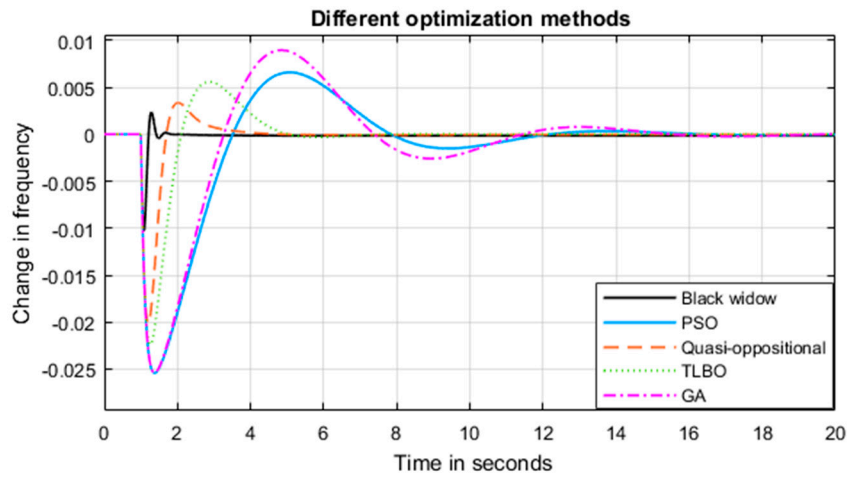


Figure 10. Change in frequency using different optimization techniques.

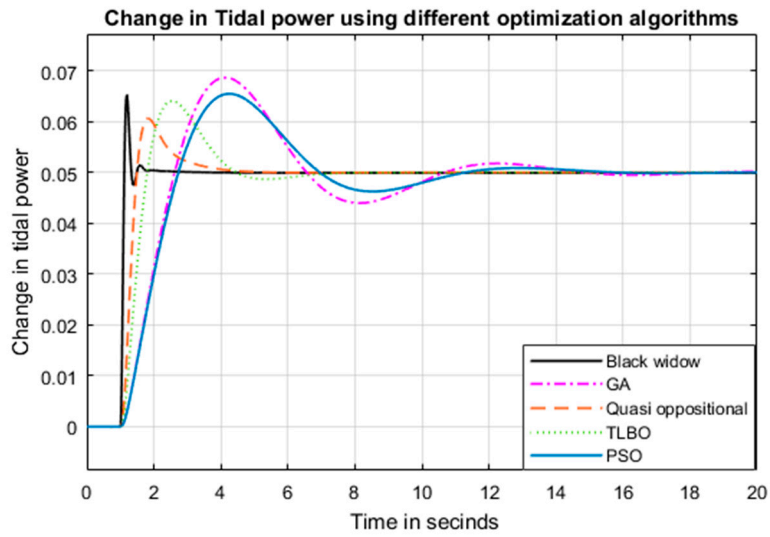


Figure 11. Change in tidal power using different optimization techniques.

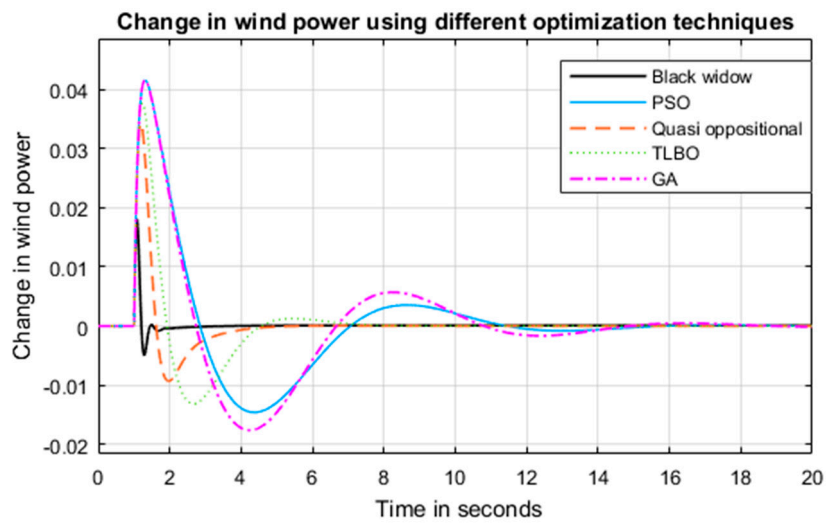


Figure 12. Change in wind power using different optimization techniques.

**Table 2.** Comparison of optimization methods.

Method	ITAE	IAE	$\int(\Delta f)^2 * 10^{-6}$	Number of Iterations	Transient Response of $\Delta f$			
					$U_{sh}$	$O_{sh}$	$t_s$	$t_p$
Black widow	0.0059	0.0011	0.39	15	-0.01	0.0025	1.75	1.5
Quasi-oppositional	0.0064	0.0016	0.42	21	-0.02	0.003	3.5	2
TLBO	0.0071	0.0019	0.48	18	-0.022	0.006	4.5	2.8
PSO	0.0085	0.0026	0.61	25	-0.025	0.007	15	4
GA	0.0089	0.0027	0.64	23	-0.025	0.009	15	4

5.1. System Performance under Test 1

In this test, the studied microgrid is subjected to a step increase in demand by 10% 1 second after starting the simulation. Four control strategies have been carried out on the system:

- Strategy a: System without supplementary control
- Strategy b: System with integrator supplementary control
- Strategy c: System with fractional integrator supplementary control
- Strategy d: System with non-linear fractional integrator supplementary control.

Figures 13–15 show the frequency deviation, change in tidal power, and change in wind power when the system is subjected to *Test 1*. The results show that the non-linear fractional integrator achieved a better performance than the fractional integrator, followed by the conventional integrator. To avoid mechanical oscillations, the optimal parameters of the supplementary control, added damping ( $D_1$ ) and added inertia ( $M$ ) in addition to the rest of the controllers of the system, are tuned at the same time to get the optimal parameters for the whole system considering the mechanical oscillations. If the integrator is not inserted in the system, there is a steady-state error and a very long settling time. System controllers and different supplementary control schemes parameters are illustrated in Table 3. Table 4 illustrates the performance of the microgrid at different frequency dependencies of the load ( $D$ ); the results show that as  $D$  increases, the performance of the microgrids gets better in terms of ITAE, IAE, and settling time: in other words, as the loads used are more frequency dependent, the microgrid performance improves.

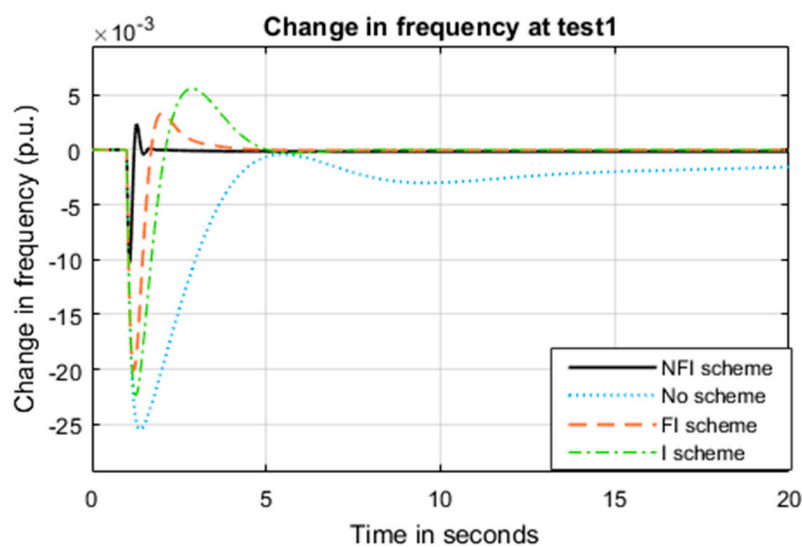


**Figure 13.** Change in frequency when the system was subjected to test 1.

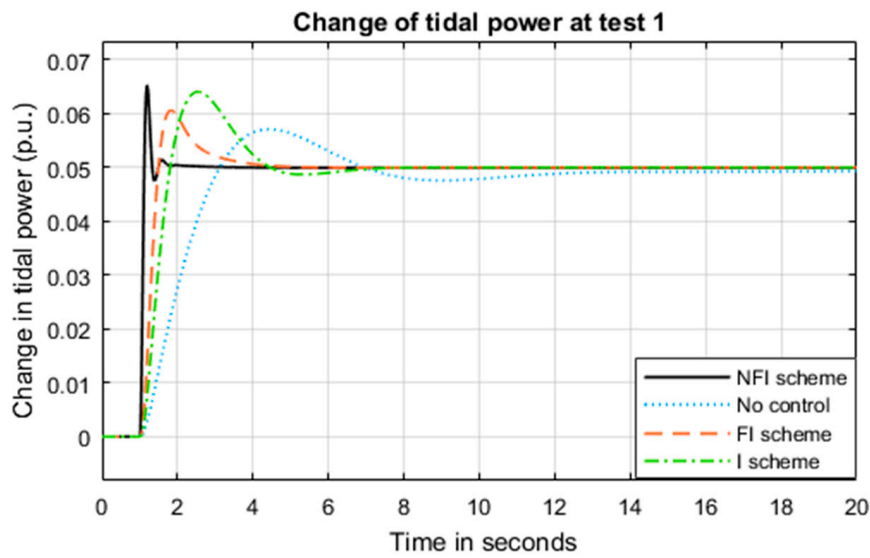


Figure 14. Change in tidal power when the system was subjected to test 1.

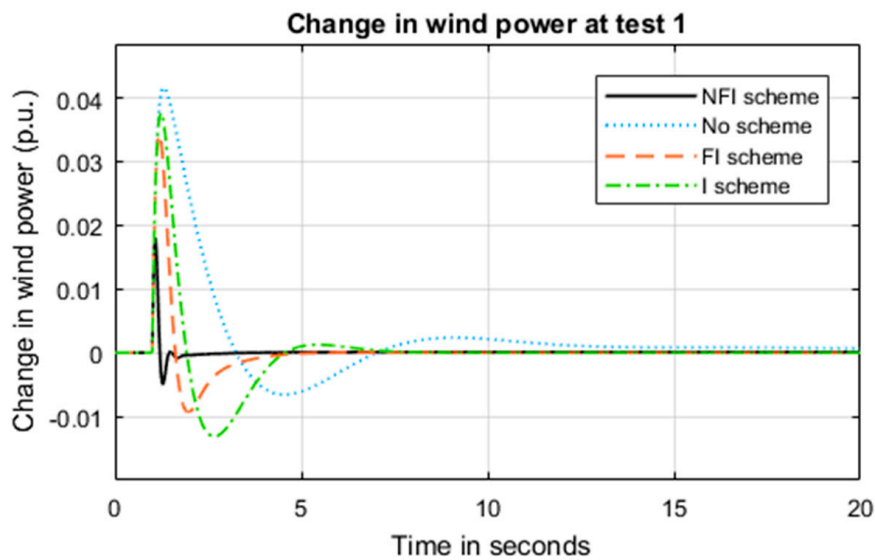


Figure 15. Change in wind power when the system was subjected to test 1.

Table 3. Microgrid control schemes parameters in test 1.

Control Scheme	$M$	$D_1$	Supplementary Control			Tidal Blade Pitch Controller			Tidal Speed Regulator			Wind Blade Pitch Controller		
			$K_I$	$\lambda$	$G$	$K_P$	$K_I$	$K_D$	$K_{\omega TP}$	$K_{\omega TI}$	$K_{\omega TD}$	$K_P$	$K_I$	$K_D$
No scheme	150	147	none	none	none	10	3	0.4	50	17	12	16	5	0.3
I scheme	122	85	10	none	none	17	14	11	14	5	4	17	1	0.2
FI scheme	146	75	7	0.43	none	11	9	0.16	6	4	1.4	8	5	2
NFI scheme	98	56	13	0.64	0.72	14	7	1.14	8	3	0.57	21	17	8

**Table 4.** Microgrid frequency indicators for different load types at test 1.

Control Scheme	$D = 0.8$			$D = 1$			$D = 1.2$			$D = 1.4$		
	ITAE	IAE	$t_s$	ITAE	IAE	$t_s$	ITAE	IAE	$t_s$	ITAE	IAE	$t_s$
No scheme	0.087	0.061	17	0.079	0.050	15	0.071	0.038	12	0.059	0.032	11
I scheme	0.064	0.052	5	0.058	0.043	4.3	0.049	0.035	3.7	0.041	0.026	3.4
FI scheme	0.053	0.039	4.2	0.041	0.031	3.9	0.036	0.024	3.1	0.023	0.017	2.8
NFI scheme	0.031	0.022	1.8	0.029	0.018	1.7	0.024	0.014	1.6	0.018	0.009	1.5

5.2. System Performance under Test 2

In this test, the studied microgrid is subjected to real-time load variations (shown in Figure 16). The same control strategies of test 1 are applied in this test. The same parameters as test 1 are kept for all controllers and integrators. The competitive profiles of frequency deviation, in addition to the change in tidal generation and change in wind generation are presented in Figure 17, Figure 18, and Figure 19, respectively. The results show that the non-linear fractional integrator has a better performance than the other control schemes.

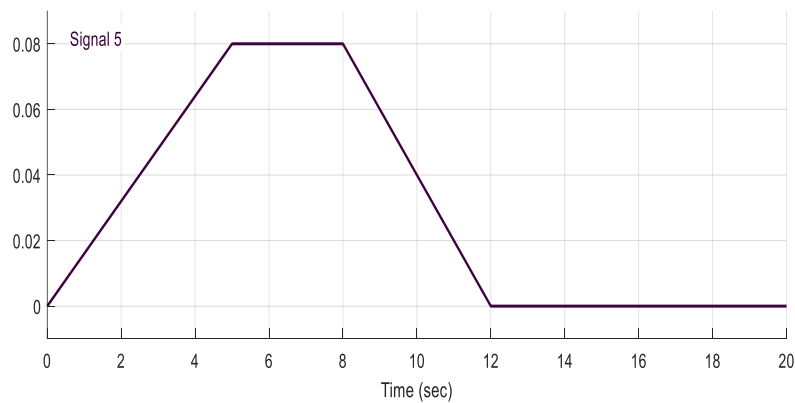


**Figure 16.** Change in demand in test 2.

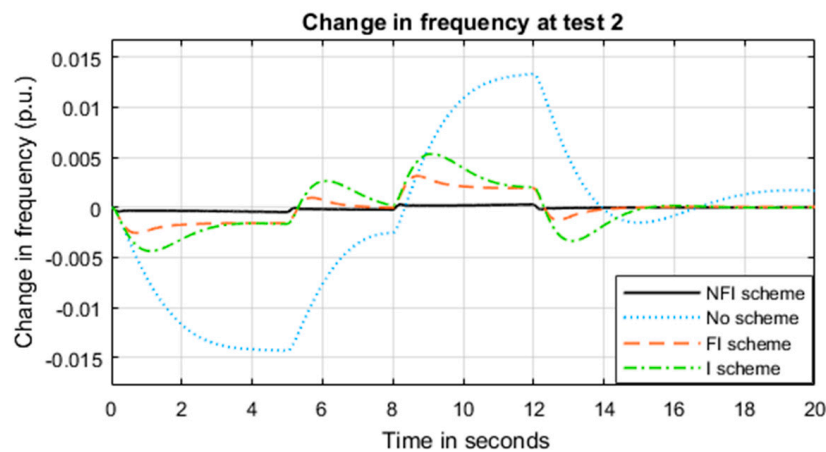


**Figure 17.** Change in frequency in test 2.

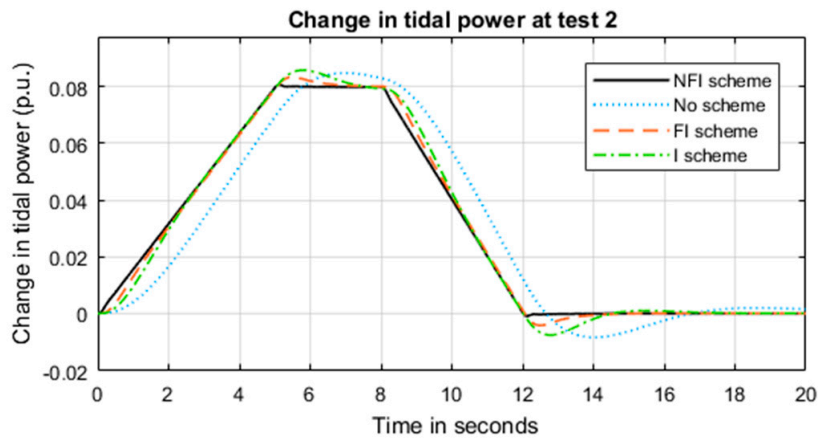


Figure 18. Change in tidal power in test 2.

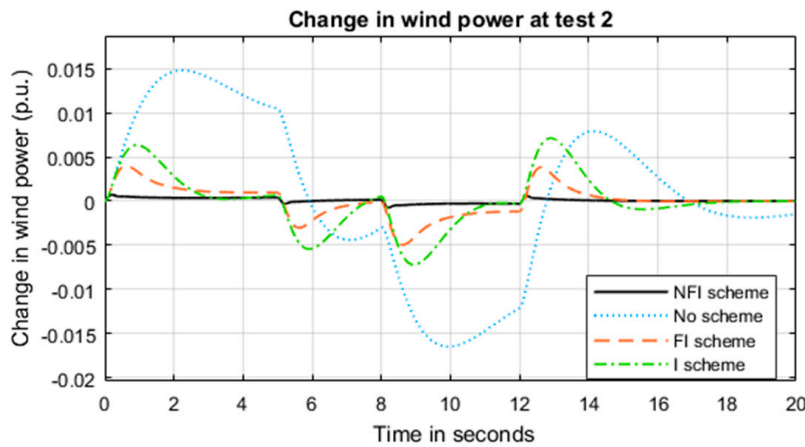


Figure 19. Change in wind power in test 2.

5.3. System Performance under Test 3

In this test, the wave system has sinusoidal power variation as expressed in the following equation [12,13].

$$\Delta P_{wave} = 0.002 \sin(4.36t) + 0.005 \sin(5.3t) - 0.01 \sin(6t) \tag{22}$$

The same parameters as test 1 are kept for all controllers and integrators. The competitive profiles of frequency deviation, in addition to change in tidal generation and change in wind generation all measured per unit (p.u.), are presented in Figure 20, Figure 21, and Figure 22, respectively. The results show that the non-linear fractional integrator has a better performance than the other control schemes.

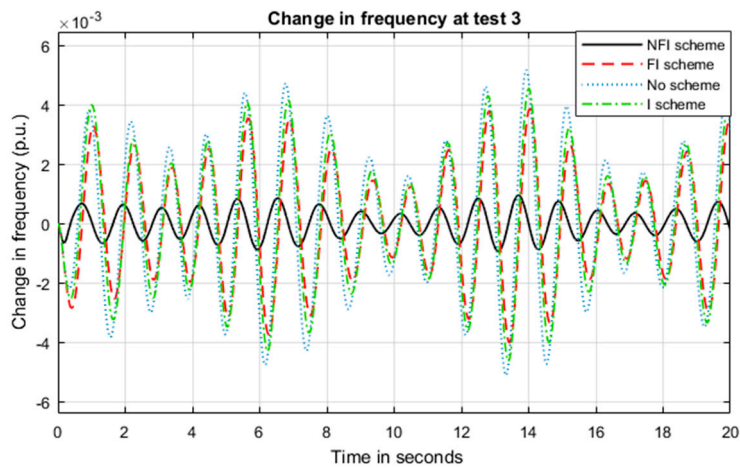


Figure 20. Change in frequency in test 3.

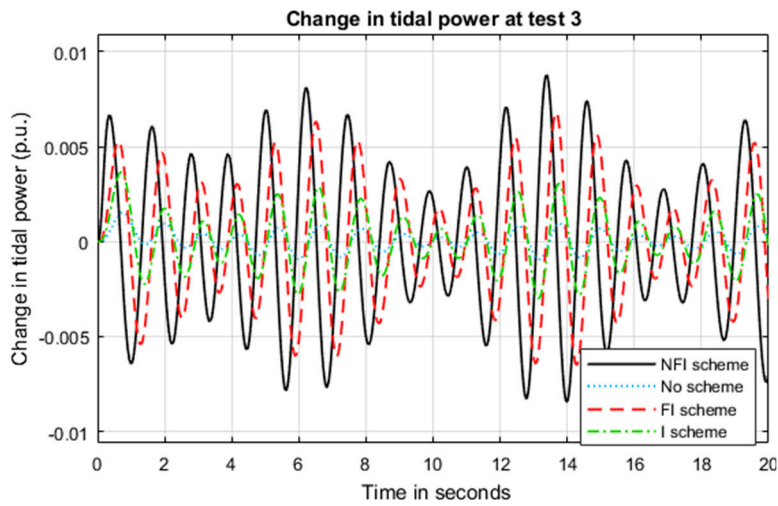


Figure 21. Change in tidal power in test 3.

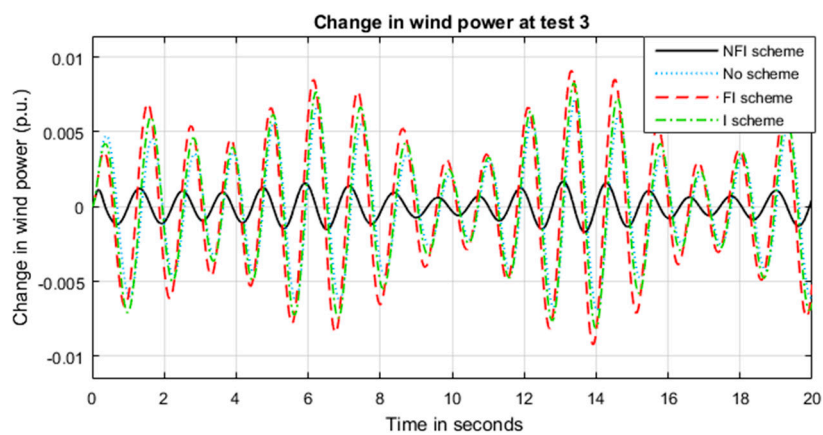


Figure 22. Change in wind power in test 3.

## 6. Conclusions

This paper has presented the load frequency control of a 100% renewable energy marine microgrid in terms of wind, tidal, and waves generators. The results show that using a tidal supplementary controller in the presence of an integrator drives the microgrid to zero steady-state frequency deviation in different operating conditions. The results show that the contribution of the tidal supplementary

controller to the load or generation variation is more effective than the wind blade pitch controller in different operating conditions. The results also proved that the proposed non-linear fractional order integrator (NFI) based supplementary control achieves better performance than fractional order integrator (FI) and conventional integrator (I) schemes in different operating conditions. The results also proved that the FI control scheme drives the system to a better performance than the I control scheme. The results also proved that the controller design using a black widow optimization algorithm drives the system to a better performance than other existing state-of-the-art algorithms, in terms of ITAE, IAE, number of iterations, and change in frequency transient response. The results also show that using an NFI control scheme will lead the system to a better performance when subjected to sinusoidal wave power generation than will FI and I control schemes. The paper presents a technique to solve the frequency deviation in sea/ocean isolated microgrid. To practically apply this technique, integration between tidal, wind and wave technologies and software and microcontroller facilities, are required.

**Author Contributions:** Conceptualization, H.H.F.; methodology, H.H.F.; software, H.H.F.; validation, H.H.F.; formal analysis, H.H.F.; investigation, H.H.F.; resources, H.H.F. and B.M.-I.; data curation, H.H.F.; writing—original draft preparation, H.H.F. and B.M.-I.; writing—review and editing, H.H.F. and B.M.-I.; visualization, H.H.F. All authors have read and agreed to the published version of the manuscript.

**Funding:** This research received no external funding.

**Conflicts of Interest:** The authors declare no conflict of interest.

## Appendix A

**Table A1.** Marine microgrid system parameters.

System	Parameters
Tidal	Capacity: 1 MW, rated rotor speed ( $\omega_r$ ) = 13 rpm, tidal speed (V) = 2.4 m/s, TSR = 6.1, rotor radius (r) = 11.5 m, rotor blades = 3, blade length = 10.6 m, rotor position = upstream, $M_T = 0.3878$ s, $T_P = 0.01$ s, $T_T = 0.08$ s, $T_w = 6$ s, angle limits: minimum = $0^\circ$ and maximum = $90^\circ$ , $d_1 = 0.18$ , $d_2 = 85$ , $d_3 = 0.38$ , $d_4 = 10.2$ , $d_5 = 6.2$ , $d_6 = 0.025$ , $d_7 = -0.043$
Wave	Capacity: 1 MW, $K_{wave} = 1$ , $T_{wave} = 0.3$ s, $T_{inv} = T_{conv} = 0.01$ s
Offshore wind	Capacity: 1 MW, $K_{p1} = 1.250$ , $K_{p2} = 1.000$ , $K_{p3} = 1.400$ , $K_{TP} = 0.0033$ , $K_{IG} = 0.9969$ , $K_{PC} = 0.0800$ , $T_{p1} = 0.6000$ s, $T_{p2} = 0.0410$ , $T_{p3} = 1.000$ , $T_W = 4.000$
Microgrid	$H = 5$ , $D = 0.8$ , $f = 50$ Hz

## References

1. Abdalla, O.H.; Fayek, H.H.; Abdel Ghany, A.M. Secondary Voltage Control Application in a Smart Grid with 100% Renewables. *Inventions* **2020**, *5*, 37. [[CrossRef](#)]
2. Fayek, H.H. Voltage and Reactive Power Control of Smart Grid. Ph.D. Thesis, Helwan University, Helwan, Egypt, February 2019.
3. Fayek, H.H. Load Frequency Control of a Power System with 100% Renewables. In Proceedings of the 2019 54th International Universities Power Engineering Conference (UPEC), Bucharest, Romania, 3–6 September 2019; pp. 1–6.
4. Rourke, F.; Boyle, F.; Reynolds, A. Tidal energy update 2009. *Appl. Energy* **2010**, *87*, 398–409. [[CrossRef](#)]
5. De Almeida, R.G.; Lopes, J.A.P. Participation of Doubly Fed Induction Wind Generators in System Frequency Regulation. *IEEE Trans. Power Syst.* **2007**, *22*, 944–950. [[CrossRef](#)]
6. Zaheeruddin; Singh, K. Primary frequency regulation of a microgrid by deloaded tidal turbines. *Soft Comput.* **2020**, *24*, 14667. [[CrossRef](#)]
7. Whitby, B.; Ugalde-Loo, C.E. Performance of Pitch and Stall Regulated Tidal Stream Turbines. *IEEE Trans. Sustain. Energy* **2013**, *5*, 64–72. [[CrossRef](#)]
8. Bryans, A.; Fox, B.; Crossley, P.; O'Malley, M. Impact of Tidal Generation on Power System Operation in Ireland. *IEEE Trans. Power Syst.* **2005**, *20*, 2034–2040. [[CrossRef](#)]

9. Mauricio, J.M.; Marano, A.; Gomez-Exposito, A.; Ramos, J.L.M. Frequency Regulation Contribution through Variable-Speed Wind Energy Conversion Systems. *IEEE Trans. Power Syst.* **2009**, *24*, 173–180. [[CrossRef](#)]
10. Da, Y.; Khaligh, A. Hybrid offshore wind and tidal turbine energy harvesting system with independently controlled rectifiers. In Proceedings of the 2009 35th Annual Conference of IEEE Industrial Electronics, Porto, Portugal, 3–5 November 2009; pp. 4577–4582.
11. Rahman, M.L.; Shirai, Y. Hybrid offshore-wind and tidal turbine (HOTT) energy conversion I (6-pulse GTO rectifier and inverter). In Proceedings of the 2008 IEEE International Conference on Sustainable Energy Technologies, Singapore, 24–27 November 2008; pp. 650–655.
12. Huang, J.; Yang, J.; Xie, D.; Wu, D. Optimal Sliding Mode Chaos Control of Direct-Drive Wave Power Converter. *IEEE Access* **2019**, *7*, 90922–90930. [[CrossRef](#)]
13. Hasanien, H.M. Transient Stability Augmentation of a Wave Energy Conversion System Using a Water Cycle Algorithm-Based Multiobjective Optimal Control Strategy. *IEEE Trans. Ind. Inform.* **2018**, *15*, 3411–3419. [[CrossRef](#)]
14. Ghoshal, S. Optimizations of PID gains by particle swarm optimizations in fuzzy based automatic generation control. *Electr. Power Syst. Res.* **2004**, *72*, 203–212. [[CrossRef](#)]
15. Das, D.C.; Roy, A.; Sinha, N. GA based frequency controller for solar thermal–diesel–wind hybrid energy generation/energy storage system. *Int. J. Electr. Power Energy Syst.* **2012**, *43*, 262–279. [[CrossRef](#)]
16. Rao, R.V.; Savsani, V.J.; Vakharia, D.P. Teaching–learning-based optimization: A novel method for constrained mechanical design optimization problems. *Comput. Des.* **2011**, *43*, 303–315. [[CrossRef](#)]
17. Pan, Q.-K.; Suganthan, P.; Tasgetiren, M.F.; Liang, J. A self-adaptive global best harmony search algorithm for continuous optimization problems. *Appl. Math. Comput.* **2010**, *216*, 830–884. [[CrossRef](#)]
18. Hayyolalam, V.; Kazem, A.A.P. Black Widow Optimization Algorithm: A novel meta-heuristic approach for solving engineering optimization problems. *Eng. Appl. Artif. Intell.* **2020**, *87*, 103249. [[CrossRef](#)]
19. Rawat, S.; Singh, S.; Gaur, K. Load frequency control of a hybrid renewable power system with fuel cell system. In Proceedings of the 2014 6th IEEE Power India International Conference (PIICON), Delhi, India, 5–7 December 2014; pp. 1–6. [[CrossRef](#)]
20. Das, D.C.; Sinha, N.; Roy, A.K. Automatic Generation Control of an Organic Rankine Cycle Solar-Thermal/Wind-Diesel Hybrid Energy System. *Energy Technol.* **2014**, *2*, 721–731. [[CrossRef](#)]
21. Fayek, H.H.; El-Zoghby, H.M.; Ghany, A.A. Design of Robust PID Controllers Using  $H_{\infty}$  Technique to Control the Frequency of Wind-Diesel-Hydro Hybrid Power System. In Proceedings of the International Conference on Electrical Engineering, San Francisco, CA, USA, 22–24 October 2014.
22. Fayek, H.H. Robust Controllers Design of Hybrid System Load Frequency Control. Master’s Thesis, Helwan University, Helwan, Egypt, 2014.
23. Fayek, H.H.; Shenouda, A. Design and Frequency Control of Small Scale Photovoltaic Hydro Pumped Storage System. In Proceedings of the 2019 IEEE 2nd International Conference on Renewable Energy and Power Engineering (REPE), Toronto, ON, Canada, 2–4 November 2019; pp. 32–37.
24. Kumar, A.; Shankar, G. Quasi-oppositional harmony search algorithm based optimal dynamic load frequency control of a hybrid tidal–diesel power generation system. *IET Gener. Transm. Distrib.* **2018**, *12*, 1099–1108. [[CrossRef](#)]
25. Veronica, A.J.; Kumar, N.S.; Gonzalez-Longatt, F. Design of Load Frequency Control for a Microgrid Using D-partition Method. *Int. J. Emerg. Electr. Power Syst.* **2020**, *21*, 20190175. [[CrossRef](#)]
26. Chen, M.-R.; Zeng, G.-Q.; Dai, Y.-X.; Lu, K.-D.; Bi, D.-Q. Fractional-Order Model Predictive Frequency Control of an Islanded Microgrid. *Energies* **2019**, *12*, 84. [[CrossRef](#)]
27. Hefiri, K.; Garrido, A.J.; Rusu, E.; Bouallègue, S.; Haggège, J.; Garrido, I. Fuzzy Supervision Based-Pitch Angle Control of a Tidal Stream Generator for a Disturbed Tidal Input. *Energies* **2018**, *11*, 2989. [[CrossRef](#)]

**Publisher’s Note:** MDPI stays neutral with regard to jurisdictional claims in published maps and institutional affiliations.



© 2020 by the authors. Licensee MDPI, Basel, Switzerland. This article is an open access article distributed under the terms and conditions of the Creative Commons Attribution (CC BY) license (<http://creativecommons.org/licenses/by/4.0/>).